Int. J. Heat Mass Transfer. Vol. 30, No. 5, pp. 881–891, 1987
Printed in Great Britain

0017–9310/87 $3.00 + 0.00

Heat and mass transfer associated with a spray drop experiencing condensation: a fully transient analysis

LIN JIE HUANG and P. S. AYYASWAMY
Department of Mechanical Engineering and Applied Mechanics, University of Pennsylvania, Philadelphia, PA 19104, U.S.A.

(*Received* 15 *April* 1986 *and in final form* 3 *September* 1986)

Abstract—The time-dependent hydrodynamics and heat/mass transport associated with condensation on a spray drop have been investigated for the Reynolds number of drop motion in the range, $Re = O(100)$. The drop environment is a mixture of saturated vapor and a noncondensable. The formulation entails a simultaneous solution of the partial-differential equations that describe the flow field and transport in the gaseous and liquid phases. The trajectory of the droplet is established by solving the relevant gravity-drag force balance equations. Results have been provided for the temporal variations of drop bulk temperatures, various drag coefficients, average condensation velocity, and average heat flux. The effect of spray angle on the drop vertical-fall height before reaching thermal equilibration with the outside environment is discussed. Results show excellent agreement with experimental data where available. New correlations for the average condensation velocity and the average heat flux associated with condensation on a moving liquid drop in the presence of a noncondensable have been provided. The correlations are thought to be of considerable usefulness in the design of direct-contact heat/mass transfer equipment.

1. INTRODUCTION

CONDENSATION on a spray of drops occurs in a wide variety of physical situations. For example, the emergency cooling sprays of nuclear reactors, air-conditioning humidifiers, direct contact condensers in thermal power plants, atmospheric studies of raindrop growth, etc. involve condensation on moving drops. The intent of the present paper is to analyze the hydrodynamics and the transport phenomena associated with condensation on a single moving drop, for a wide range of condensation rates, drop diameters, initial velocities, and spray angles. Although realistic situations demand the consideration of a spectrum of moving drops of various sizes, still it is important to first gain a fundamental understanding of the single-drop problem before a more general analysis is attempted.

There are many studies in the literature that involve heat and mass transfer and/or hydrodynamics of drop motion [1]. Specifically, with regard to condensation on drops, stationary drops have been studied in refs. [2–4]. The growth rate of a water drop in a pure steam environment has been experimentally investigated in ref. [5]. The condensation heat-transfer rates for droplets moving in air—steam mixtures have been predicted using standard heat-transfer correlations in ref. [6]. In ref. [7], the authors have provided the experimentally recorded temperature–time history of a water drop experiencing condensation in a forced flow of steam and air. Condensation on slowly moving drops has been theoretically examined in refs. [8–10]. Condensation in the vicinity of the front stagnation point of a drop in high-Reynolds number motion has been investigated in refs. [11, 12]. Results for quasi-steady condensation heat and mass transfer appropriate to the intermediate Reynolds number range of drop motion are given in refs. [13, 14]. A hybrid finite-difference scheme that is suitable for solving condensation problems associated with a single drop has been described in ref. [15].

In this paper we examine condensation on a spherical drop that is translating with a flow Reynolds number $Re = O(100)$. A fully transient analysis is described. The drop environment is a saturated mixture of condensable vapor and a non-condensable gas. Condensation on the entire drop surface has been considered. The flow problems inside and outside the drop have been simultaneously treated. A constant-property model describes the transport in the gaseous phase. The flow solutions and transport rates to the drop are obtained in terms of two non-dimensional parameters (one, Re, representing the flow conditions, and the other, W, representing the thermodynamic conditions). The time-dependent partial differential equations for the gaseous phase are solved by a hybrid finite-difference scheme [15]. The scheme involves central-differencing near the drop surface and upwind differencing in the far field. It provides accurate results near the drop surface while guaranteeing numerical stability in the far field. The drop interior, both the flow and heat-up, is also treated in a fully transient manner.

2. PHYSICAL DESCRIPTION

Consider the introduction of a cold water drop of radius R_0 and initial bulk temperature T_0 into an

NOMENCLATURE

c_p	specific heat
D	drag coefficient; drop diameter
D_{12}	binary diffusion coefficient
$\mathbf{e}$	unit vector
Eo	Eötvös number, $g\Delta\rho D^2/\sigma$
H	vertical-fall height
Ja_g	Jakob number, $c_{pg}(T_\infty - T_0)/\lambda$
$\mathbf{i}$	unit vector in x-direction
$\mathbf{j}$	unit vector in y-direction
k	thermal conductivity
Le	Lewis number, α/D_{12}
m_1	non-condensable mass fraction
p_∞	far-stream pressure
Pe	Peclet number, $U_\infty D/\alpha$ or $U_\infty D/D_{12}$
q	heat flux
r	radial coordinate
R	instantaneous radius of the drop
R_0	initial radius of the drop
$\hat{R}$	instantaneous dimensionless radius of the drop, R/R_0
$\dot{R}$	dimensionless rate of change of drop radius (scaled by U_∞)
R_∞	radius of the outer boundary in the numerical calculation
Re	Reynolds number, $U_\infty D/\nu$
Sc	Schmidt number, ν/D_{12}
t	time
T	temperature
T_b	instantaneous bulk temperature of the drop
T_s	surface temperature of the drop
$\mathbf{u}$	velocity
$\hat{u}_c$	dimensionless condensation velocity
u_c	dimensionless condensation velocity at the drop surface scaled by $D_{12}/2R$
$\mathbf{U}_0$	initial velocity of drop
$\mathbf{U}_\infty$	far-stream translational velocity
u_r, u_θ	velocity components
w_1	normalized mass fraction
W	condensation parameter, $1 - m_{1,\infty}/m_{1,s}$
z	transformed radial coordinate, $\ln r$.

Greek symbols

α	thermal diffusivity
β	instantaneous angle of drop trajectory
$\Delta\rho$	density difference between drop and gaseous phase
ζ	vorticity
θ	polar angle
θ_b	dimensionless bulk temperature
λ	latent heat of condensation
μ	dynamic viscosity
ν	kinematic viscosity
ρ	density
σ	surface tension
ϕ	azimuthal angle
ψ	stream function.

Subscripts

av	average
c	condensation
f	friction
g	gas phase
h	horizontal
l	liquid phase
m	mass transfer
p	pressure
s	drop surface
t	thermal, total
v	vertical
0	at initial time; stagnant drop
1	noncondensable
∞	far-stream.

Superscripts

$\bar{}$	average
*	dimensionless quantity.

environment consisting of a mixture of vapor (steam) and non-condensable (air). The droplet is projected with an initial velocity $\mathbf{U}_0$ and at an angle β_0 with respect to the vertical direction (Fig. 1). The total pressure p_∞ and temperature T_∞ of the saturated mixture in the drop environment are taken to be prescribed. The drop is colder than its environment ($T_0 < T_\infty$) and condensation occurs on the drop surface. The shear stress at the interface due to drop translation will initiate liquid circulation inside the drop. The heat deposited in the drop surface will heat up the drop liquid.

Let the instantaneous translational velocity of the drop be $\mathbf{U}_\infty$. We consider a coordinate frame that coincides with the drop center and moves with this instantaneous velocity $\mathbf{U}_\infty$ (Fig. 1). The instantaneous gaseous phase Reynolds number of translation (hereinafter referred as $Re_g = U_\infty 2R/\nu_g$) is taken to be $O(100)$, but less than, say, 500. For $Re_g \gtrsim 500$ flow instabilities such as drop oscillations and vortex shedding are known to occur. In our analysis the drop deformation due both to inertial effects (Weber number We) and to hydrostatic-pressure variation (Eötvös number Eo) are assumed to be small. We consider water drops of size 1 mm diameter or less ($Eo < 0.4$ and $We < 0.3$). Next consider the circulation inside the drop. For the range of Re_g considered in the present study, the circulation Reynolds number Re_l based on U_s, the maximum circulation velocity at the drop surface, may be shown to be of $O(10^2)$

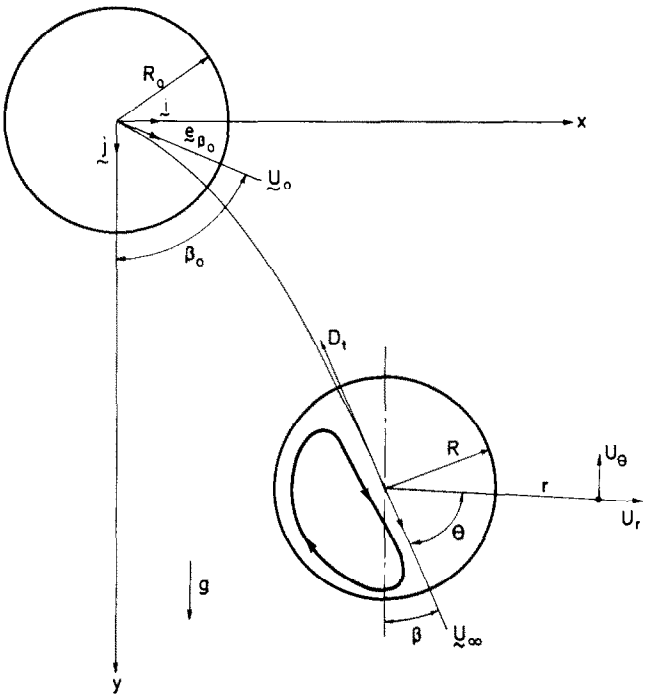

FIG. 1. Geometry of the problem.

[13]. The flow pattern inside the drop resembles Hill's spherical vortex [13]. Since the liquid Prandtl number $Pr_l (= \nu_l/\alpha_l)$ is $O(10)$, the Peclet number $Pe_l (= U_l 2R/\alpha_l)$, for heat transport inside the drop is $O(10^3)$. ν and α are the kinematic viscosity and thermal diffusivity, respectively.

Condensation causes a radially inward flow towards the drop surface. The non-zero mass flux at the interface alters the translational flow field and modifies the drag on the drop. Also, the radial flow leads to a build-up of the non-condensable concentration near the drop surface above that in the free stream. The accumulation results in a mass-transfer resistance and a consequent reduction in the transport rates.

For $Re_g = O(10^2)$ flow separates on the rear of the drop. A recirculating wake is formed and the radial flow due to condensation reduces the wake size [13]. In this analysis, the effects of non-condensable accumulation, liquid circulation and external-flow separation have been taken into account in the development of the results.

3. DROP-TRAJECTORY DETERMINATION

Let U_h and U_v be the instantaneous horizontal and vertical components of the drop velocity such that $\mathbf{U}_\infty = \mathbf{i}U_h + \mathbf{j}U_v$. The dimensionless equations of motion that govern the drop trajectory may be shown to be (asterisks indicate dimensionless quantities):

$$\frac{dU_v^*}{dt^*} = \frac{R^2 g}{\alpha_g U_0} - \frac{3}{16}\frac{\rho_g}{\rho_l} Pe_g D_t \frac{U_\infty}{U_0}\cos\beta \qquad (1)$$

and

$$\frac{dU_h^*}{dt^*} = -\frac{3}{16}\frac{\rho_g}{\rho_l} Pe_g D_t \frac{U_\infty}{U_0}\sin\beta \qquad (2)$$

where R is the instantaneous radius of the drop, the dimensionless velocity components $U_v^* = U_v/U_0$, $U_h^* = U_h/U_0$, t^* is dimensionless time $\left(= \int_0^t \frac{\alpha_g\, dt}{R^2}\right)$, g is the acceleration due to gravity, α_g is the thermal diffusivity of the gaseous phase, ρ_g and ρ_l are the densities in the gaseous and liquid phases, D_t is the instantaneous total-drag coefficient, and β is the instantaneous direction.

The instantaneous total-drag coefficient

$$D_t = D_p + D_f + D_c \qquad (3)$$

where D_p, D_f and D_c are the pressure-drag, friction-drag and condensation-drag coefficients, respectively [13]. The pressure-drag coefficient is

$$D_p = \int_0^\pi p_{g,s}^* \sin 2\theta\, d\theta \qquad (4)$$

where the dimensionless pressure is

$$p_{g,s}^* = \frac{(p_{g,s}(\theta) - p_\infty)}{\frac{1}{2}\rho_g U_\infty^2}. \qquad (5)$$

The surface pressure profile is given by $p_{g,s}(\theta)$. The friction-drag coefficient is defined by

$$D_f = \frac{8}{Re_g}\int_0^\pi \sigma^* \sin\theta - 2\left.\frac{\partial u_{g,r}^*}{\partial r^*}\right|_{r^*=1} \cos\theta \sin\theta\, d\theta. \qquad (6)$$

In equation (6), the dimensionless surface shear stress σ^* and radius r^* are

$$\sigma^* = \frac{\sigma}{\mu_g U_\infty / R} \text{ and } r^* = r/R. \tag{7}$$

The surface shear stress σ itself may be expressed as

$$\sigma = \mu_g \left[r \frac{\partial}{\partial r} \frac{u_{g,\theta}}{r} + \frac{1}{r} \frac{\partial u_{g,r}}{\partial \theta} \right]_{r=R}. \tag{8}$$

In equations (6) and (8), the r and θ components of the mass average velocity, $\mathbf{u}_g$, for the binary mixture of air and water vapor are represented by $u_{g,r}$ and $u_{g,\theta}$, respectively. These are scaled by U_∞ to get $u^*_{g,r}$ and $u^*_{g,\theta}$.

The condensation drag, D_c, arises owing to the momentum associated with the radial flow and is given by

$$D_c = 4 \int_0^\pi \left[\hat{u}_c^* \cos\theta - u_\theta^* \sin\theta \right] \hat{u}_c^* \sin\theta \, d\theta. \tag{9}$$

The dimensionless condensation velocity $\hat{u}_c^*$ and the surface velocity u_θ^* are

$$\hat{u}_c^* = u^*_{g,r}\Big|_{r^*=1} \text{ and } u_\theta^* = u^*_{g,\theta}\Big|_{r^*=1}. \tag{10}$$

4. GAS PHASE EQUATIONS

The non-dimensional equations for the gaseous phase (subscript g refers to the mixture, 1 to the noncondensable, 2 to vapor, and omitting the asterisks for convenience) are

$$\nabla \cdot \mathbf{u}_g = 0 \tag{11}$$

$$\frac{\partial \mathbf{u}_g}{\partial t} + \frac{1}{2} Pe_{g,t} \mathbf{u}_g \cdot \nabla \mathbf{u}_g = -\frac{1}{4} Pe_{g,t} \nabla P_g + Pr_g \nabla^2 \mathbf{u}_g \tag{12}$$

$$\frac{\partial T_g}{\partial t} + \frac{1}{2} Pe_{g,t} \mathbf{u}_g \cdot \nabla T_g = \nabla^2 T_g \tag{13}$$

$$\frac{\partial w_1}{\partial t} + \frac{1}{2} Pe_{g,m} \mathbf{u}_g \cdot \nabla w_1 = \nabla^2 w_1. \tag{14}$$

The pressure p_g is scaled just as the surface value $p_{g,s}$. The temperature T_g and mass fraction m_1 have been nondimensionalized as follows:

$$T_g^* = (T_g - T_\infty)/(T_0 - T_\infty),$$

$$\text{and } w_1^* = (m_1 - m_{1,\infty})/(m_{1,0} - m_{1,\infty}).$$

The Peclet and Prandtl numbers are

$$Pe_{g,t} = \frac{U_\infty 2R}{\alpha_g}, \qquad Pe_{g,m} = \frac{U_\infty 2R}{D_{12}}, \qquad Pr_g = \frac{\nu_g}{\alpha_g}$$

where D is the mass diffusivity.

5. LIQUID PHASE EQUATIONS

The non-dimensional equations for the liquid phase (dropping asterisks for convenience) are

$$\nabla \cdot \mathbf{u}_l = 0 \tag{15}$$

$$\frac{\partial \mathbf{u}_l}{\partial t} + \frac{1}{2} Pe_l \mathbf{u}_l \cdot \nabla \mathbf{u}_l = -\frac{1}{4} Pe_l \nabla P_l + Pr_l \nabla^2 \mathbf{u}_l \tag{16}$$

$$\frac{\partial T_l}{\partial t} + \frac{1}{2} Pe_l \mathbf{u}_l \cdot \nabla T_l = \nabla^2 T_l \tag{17}$$

where the velocity $\mathbf{u}_l$ has been scaled by U_∞, pressure $p_l^* = (p_l - p_\infty)\Big/\frac{1}{2}\rho_l U_\infty^2$, $T_l^* = (T_l - T_\infty)/(T_0 - T_\infty)$, $Re_l = U_\infty 2R/\nu_l$, time $t^* = \int_0^t \frac{\alpha_l \, dt}{R^2}$, and T_0 is the initial bulk temperature of the drop.

6. INITIAL AND BOUNDARY CONDITIONS

The initial conditions are:

$$\left.\begin{aligned} \mathbf{u}_g = \mathbf{e}_{\beta_0}, \mathbf{u}_l = 0 \\ T_g = w_1 = 1 \text{ for } r > 1, T_l = 1 \end{aligned}\right\} t = 0^+ \tag{18}$$

where $\mathbf{e}_{\beta_0}$ is the unit vector along β_0.

At the interface ($r = 1$):

Continuity of tangential velocity

$$u_{g,\theta} = u_{l,\theta} = u_\theta. \tag{19}$$

Continuity of shear stress

$$r \frac{\partial}{\partial r} \frac{u_{g,\theta}}{r} + \frac{1}{r} \frac{\partial u_{g,r}}{\partial \theta} = \frac{\mu_l}{\mu_g} \left[r \frac{\partial}{\partial r} \frac{u_{l,\theta}}{r} + \frac{1}{r} \frac{\partial u_{l,r}}{\partial \theta} \right]. \tag{20}$$

Continuity of mass flux

$$\rho_g (u_{g,r} - \dot{R}) = \rho_l (u_{l,r} - \dot{R}) \tag{21}$$

where $\dot{R}$ is the growth rate of the drop.

Impermeability of the noncondensable

$$\frac{2W}{Pe_{g,m}} \frac{\partial w_1}{\partial r} = \hat{u}_c = \frac{u_c}{Pe_{g,m}} = u_{g,r}\Big|_{r=1} \tag{22}$$

where u_c^* is the non-dimensional condensation velocity and is given by $u_c^* = u_c/(D_{12}/2R)$. The parameter W referred to as the condensation parameter is given by $W = 1 - m_{1,\infty}/m_{1,s}$, and it is a function of the thermodynamic conditions p_∞, T_∞ and T_s. W varies from 0 to 1. The limit zero corresponds to a non-condensing situation and $W = 1$ to a pure vapor environment.

Temperature continuity

$$T_g = T_l. \tag{23}$$

Heat continuity

$$Ja_g \frac{\partial T_g}{\partial r} + \frac{1}{2Le_g}\left[u_c + \frac{\rho_g \bar{u}_c}{\rho_l - \rho_g}\right] = q_s \quad (24)$$

where the Jakob number Ja_g is given by $Ja_g = c_{pg}(T_\infty - T_0)/\lambda$, $Le_g = \alpha_g/D_{12}$ is the Lewis number for the gaseous phase, and the non-dimensional heat flux is given by $q_s^* = q_s R/\rho_g \alpha_g \lambda$. The latent heat of condensation is λ and the specific heat is c_p. The quantity $\bar{u}_c$ is the average value of u_c and is given by

$$\bar{u}_c = \frac{1}{2}\int_0^\pi u_c \sin\theta \, d\theta. \quad (25)$$

The normalized mass fraction at the interface

$$w_l = w_s. \quad (26)$$

Far-stream conditions ($r \to \infty$):
Uniform velocity:

$$\mathbf{u}_g = \mathbf{e}_\beta \quad (27)$$

where $\mathbf{e}_\beta$ is the unit vector along β at any instant of time. The bulk mixture conditions are

$$T_g = p_g = w_l = 0. \quad (28)$$

Axisymmetric conditions at $\theta = 0$ *and* $\theta = \pi$:

$$u_{g,\theta} = \frac{\partial u_{g,r}}{\partial \theta} = \frac{\partial p_g}{\partial \theta} = \frac{\partial T_g}{\partial \theta} = \frac{\partial w_l}{\partial \theta} = 0 \quad (29)$$

$$u_{l,\theta} = \frac{\partial u_{l,r}}{\partial \theta} = \frac{\partial p_l}{\partial \theta} = 0. \quad (30)$$

7. NUMERICAL PROCEDURE

The governing equations and boundary conditions are transformed in terms of the dimensionless stream function ψ (scaled with $U_\infty R^2$) and vorticity ζ (scaled with U_∞/R). In spherical coordinates (Fig. 1) the stream function and vorticity are

$$\mathbf{u}_g = \nabla \times \left[-\frac{\psi_g}{r\sin\theta}\mathbf{e}_\varphi\right], \zeta_g \mathbf{e}_\phi = \nabla \times \mathbf{u}_g \quad (31)$$

and

$$\mathbf{u}_l = \nabla \times \left[-\frac{\psi_l}{r\sin\theta}\mathbf{e}_\phi\right], \zeta_l \mathbf{e}_\phi = \nabla \times \mathbf{u}_l \quad (32)$$

where $\mathbf{e}_\phi$ is the unit vector in the ϕ-direction.

The solution domain is divided into a grid with a variable step size. A fine spacing is employed near the drop, where the gradients are steep. A coarse spacing is adequate in the far stream, where the gradients are weak. An exponential grid spacing is generated by making a transformation $r = e^z$, and considering equal spacing in z. A constant angular step size is used in the θ coordinate. Typically, $\Delta z = 0.025$, $\Delta\theta = 2°$, and a grid with 91 × 91 exterior nodes and 51 × 91 interior nodes have been used. The far-stream conditions are specified on a large but finite spherical surface of radius R_∞ [13]. To predict the transport to the drop accurately and computationally economically, a hybrid finite-difference scheme is employed [15].

A Crank–Nicolson procedure is used to evaluate the transient heat-up of the drop interior [15]. The spatial derivatives are also central differenced. The difference equations are arranged in a tri-diagonal matrix form and a computationally inexpensive tri-diagonal matrix solver algorithm is employed.

The non-linear, algebraic difference equations resulting from the numerical procedures are solved iteratively starting from suitable guess solutions. Computations are carried out until changes in the predicted transport quantities are less than 10^{-7} (absolute error) or less than 0.1% (relative error) between successive iterations. The time for a typical computer run, involving one combination of Re_g and W is of the order of 30 min on the IBM 4143 computer.

8. RESULTS AND DISCUSSION

In Fig. 2 the comparisons between our numerical results and some experimental data [7] for the dimensionless, instantaneous drop bulk temperature as a function of time, t, are shown. We define, $\theta_b = (T_b - T_0)/(T_\infty - T_0)$, where the instantaneous bulk temperature $T_b = (1/v)\int T_l \, dv$ and v is the instantaneous drop volume. The comparisons are for two situations reported in experimental studies: (i) $R_0 = 1.45$ mm, $U_\infty = 1.91\,\mathrm{m\,s^{-1}}$, $T_\infty = 80°C$, $p_\infty = 1$ bar and $T_0 = 16°C$ ($Re_g \approx 265$); and (ii) $R_0 = 1.4$ mm, $U_\infty = 1.68\,\mathrm{m\,s^{-1}}$, $T_\infty = 72.5°C$, $p_\infty = 1$ bar (or the far-stream volume fraction of stream $x_s = 35\%$) and $T_0 = 18°C$ ($Re_g \approx 225$). The drop bulk temperatures are seen to be predicted excellently. The figure also shows that, for larger non-condensable fraction in the bulk, the drop heat-up rate is slower. This illustrates the effect of the gas-phase resistance.

Figure 3 shows the temporal variation of Re_g, D_f, D_c, D_p and D_t for a moving liquid drop experiencing condensation. The Re_g decreases because of a decrease in the instantaneous translational velocity $\mathbf{U}_\infty(t)$. The decrease in $\mathbf{U}_\infty$ is due to the deceleration (dU_v/dt) in the gravity-drag force balance equation (1). For small t, (dU_v/dt) is large and negative. The Re_g decreases rapidly in this period. With increasing t, the contribution from the total-drag force term in the balance becomes progressively smaller since $U_\infty(t)$ continuously decreases. The instantaneous Reynolds number changes slowly. Eventually, when the drop thermally equilibrates with the outside environment, the condensation will cease and the drop will translate at a fixed terminal velocity. The friction drag coefficient, D_f, decreases with time (although in Fig. 3, this decrease appears to be small, it must be remembered that D_f is scaled by U_∞^2). The decrease in D_f is due to the reduced surface shear stress that accompanies an

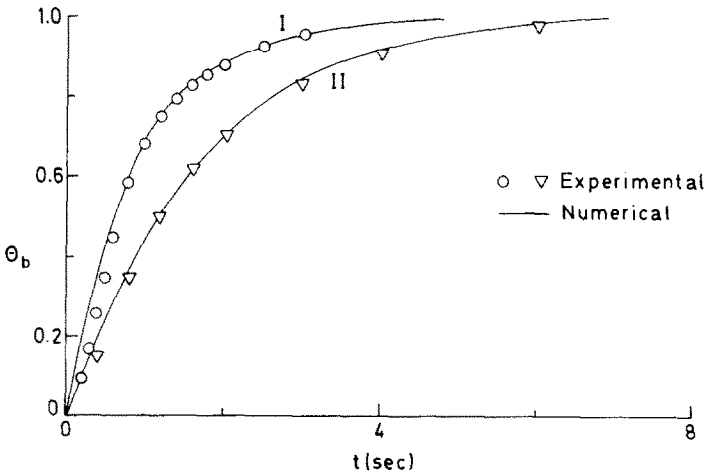

FIG. 2. The variation of drop bulk temperature with time. Comparison of numerical results with experimental data. $p_\infty = 1$ bar. I, $R_0 = 1.45$ mm, $U_\infty = 1.91\,\mathrm{m\,s^{-1}}$, $T_\infty = 80°C$, $T_0 = 16°C$; II, $R_0 = 1.40$ mm, $U_\infty = 1.68\,\mathrm{m\,s^{-1}}$, $T_\infty = 72.5°C$, $T_0 = 18°C$.

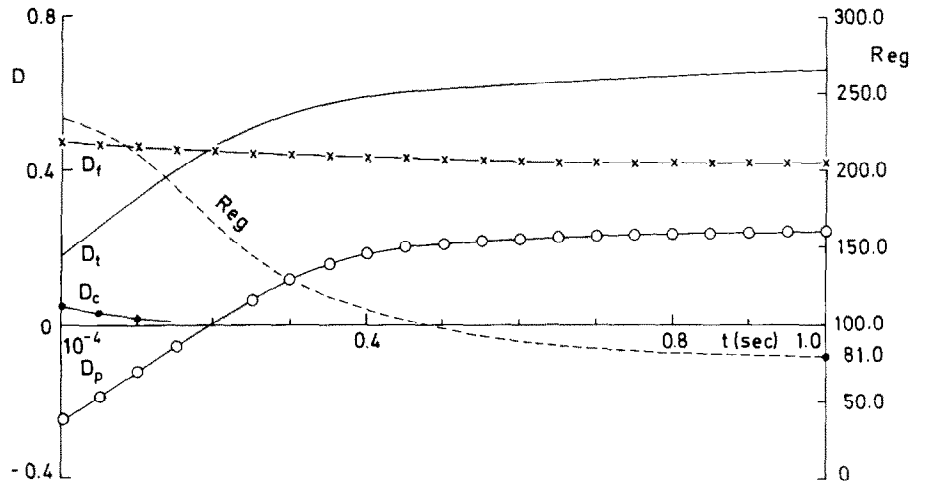

FIG. 3. The variation of Re_g, D_f, D_p, D_c and D_t with time for a vertically falling drop. $p_\infty = 300\,\mathrm{kPa}$, $T_\infty = 120°C$, $R_0 = 250\,\mu\mathrm{m}$, $W_0 = 0.54$, $T_0 = 37°C$, $U_0 = 10\,\mathrm{m\,s^{-1}}$, $Re_{g0} = 232$, $\beta_0 = 0\,\mathrm{deg}$.

increasingly weakening condensation field. We note that with increasing t, the bulk and surface temperatures of the drop increase and the thermal driving force $(T_\infty - T_s)$ keeps getting smaller, and the associated condensation field gets weaker. The condensation drag, D_c, also decreases with time. This is because the momentum transfer associated with the radial flow induced by condensation decreases with increasing time since the field itself keeps getting weaker. The variation of the pressure-drag coefficient, D_p, is somewhat complicated. The pressure-drag for a drop experiencing condensation is directly related to the pressure recovery in the rear of the drop [13]. Unlike the circumstance involving a moving solid sphere or a moving liquid drop not experiencing condensation, there is large pressure recovery in the rear of a liquid drop moving in the presence of a condensing field. With strong condensation, the wake volume is significantly reduced and the pressure-drag coefficient decreases. In particular, for the parameters used in Fig. 3, D_p is negative during the initial transient period. With increasing t and decreasing condensation, there is less pressure recovery, the D_p becomes positive and there is increased pressure drag. The variation of the total-drag coefficient, D_t, which is the sum of D_f, D_p and D_c, is thus seen to be rather complicated in a condensing situation. For the parameters used in Fig. 3, D_t is mainly controlled by the variations in D_p and D_f. As the drop approaches thermal equilibration with the outside, $D_c \to 0$, both D_f and D_p become essentially constant. The D_t becomes constant and is appropriate for a liquid drop translating at its terminal velocity without experiencing any condensation. At very high levels of condensation (say $W \sim 0.9$), the total-drag coefficient D_t may become small enough because of a large negative D_p, so that a drop of suitable size may actually accelerate in the early transient period before decelerating. This phen-

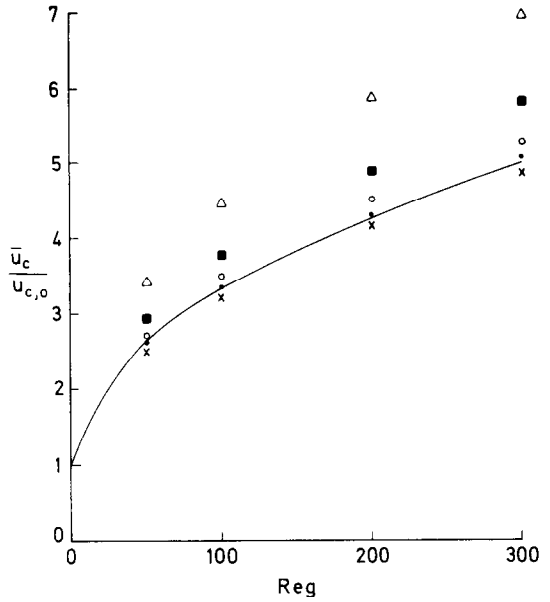

FIG. 4. The variation of $\bar{u}_c/u_{c,0}$ with Re_g and W. Comparison between numerical results and experimental correlations. $\beta_0 = 0.0$ deg., $T_0 = 37°C$, $p_\infty = 300$ kPa. ——, Experimental correlation for low W. Present work: ▲, $W = 0.9$; ○, $W = 0.5$; ×, $W = 0.1$; ■, $W = 0.7$; ●, $W = 0.3$.

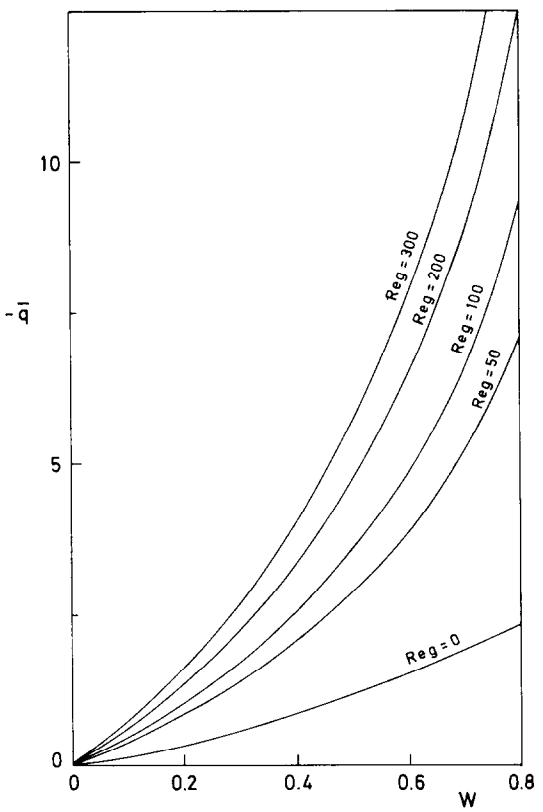

FIG. 5. The variation of average heat flux $\bar{q}$ with Re_g and W. $R_0 = 250\,\mu$m, $p_\infty = 300$ kPa, $T_\infty = 120°C$.

omenon is discussed elsewhere [16].

Figure 4 is a plot of the ratio $\bar{u}_c/u_{c,0}$ for various Re_g and W. The graph depicts the enhancement in condensation rate due to drop translation. For small values of W(large $m_{1,\infty}$ and/or a small thermal driving force $\Delta T = T_\infty - T_s$), the radial velocity induced by condensation is small. In such circumstances, the mass-transfer resistance offered by the noncondensable is essentially controlled by the translational flow field characterized by Re_g. In the figure this feature is noted for $W = 0.1$ and 0.3. The graph also shows an excellent comparison between our numerical results and an experimental correlation applicable for low-W situations [17–19]. For low rates of condensation, $\bar{u}_c$ may be predicted by

$$\bar{u}_c/u_{c,0} = 1 + 0.276 Re_g^{1/2} Sc^{1/3} \tag{33}$$

where $u_{c,0}$ is the non-dimensional condensation velocity for a stagnant drop. The solid line in the figure corresponds to this experimental correlation. For high values of W the effect of the radial flow on transport becomes significant. Based on our numerical results, we propose a new correlation of the form

$$\frac{\bar{u}_c}{u_{c,0}} = 1 + 0.261 Re_g^{1/2} Sc^{1/3}(1 - W)^{-1/5} \tag{34}$$

for $W < 1$. It may be shown [13] that in equation (34)

$$u_{c,0} = 2\ln(1 - W) \tag{35}$$

for $W < 1$.

In Fig. 5, the variation of the dimensionless average heat flux $\bar{q}$ with Re_g and W are shown. We define $\bar{q}$ as

$$\bar{q} = \frac{1}{2}\int_0^\pi q_s \sin\theta \, d\theta. \tag{36}$$

In the figure the parameters R_0, p_∞, and T_∞ are given ($m_{1,\infty}$ is prescribed). The major contribution to the interfacial heat flux comes from the latent heat of the condensing mass. The heat flux $\bar{q}$ increases in proportion to $\ln(1 - W)$ and $Re_g^{1/2}$. Based on our numerical calculations, we propose a new correlation to the dimensionless surface average heat flux for a moving drop experiencing condensation, taking into account the presence of a noncondensable, of the form

$$\bar{q} = \frac{\bar{u}_c}{2\,Le} \tag{37}$$

for $W < 1$ where $\bar{u}_c$ is given by equation (34). The use of the correlations is straightforward. For given T_0, T_∞, p_∞, U_0, β_0, and R_0, we calculate W, Re_{g0} and Sc and Le numbers. The correlations are employed to produce $\bar{q}$ and $\bar{u}_c$. The total-drag coefficient, D_t, is estimated from the correlation described in ref. [13]. The gaseous phase solutions are, therefore, essentially known to start the numerical solution. Subsequently, the trajectory equations (1) and (2), and the equation

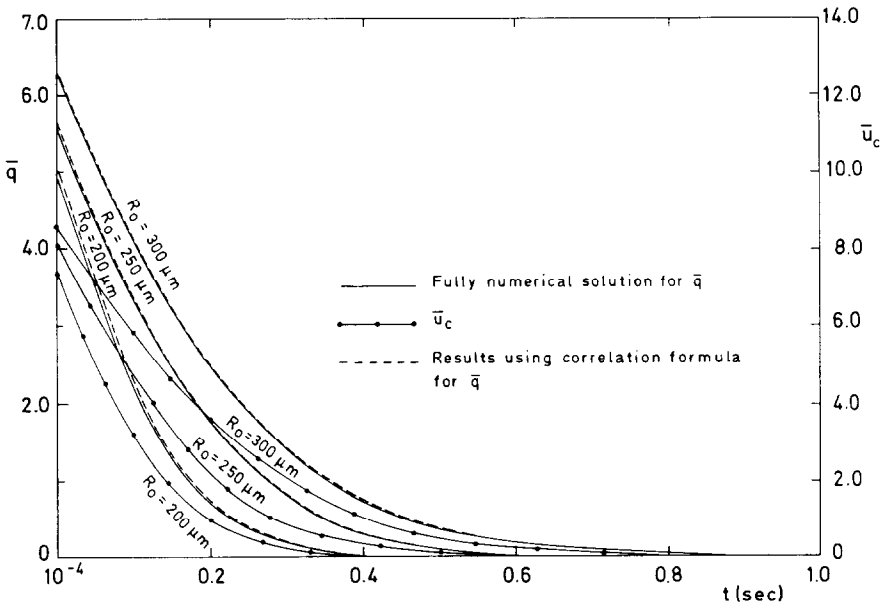

FIG. 6. $\bar{q}$ and $\bar{u}_c$ with time for falling drops of various sizes. $p_\infty = 300\,\text{kPa}$, $T_\infty = 120°\text{C}$, $U_0 = 10\,\text{m s}^{-1}$, $T_0 = 37°\text{C}$, $\beta_0 = 0.0\,\text{deg.}$, $W_0 = 0.54$.

for the transient heat up of the drop interior, equation (17), are solved subject to the initial and boundary conditions appropriate for the liquid phase. This solution procedure is facilitated by noting that in equation (17)

$$u_{1,r} \simeq 0.1(1 - r^2)\cos\theta \tag{38}$$

and

$$u_{1,\theta} \simeq 0.1(1 - 2r^2)\sin\theta. \tag{39}$$

The factor 0.1 approximately accounts for the effect of liquid viscosity on the strength of Hill's spherical vortex solution in the intermediate Reynolds number range of drop motion [11]. Repeated iterations yield the desired time history. With the use of the correlation, the time required for a typical computer run, involving one combination of Re_g and W, is of the order of a few minutes on the IBM 4143 machine. Further simplifications in the numerical procedure may be implemented if we observe that the stream surfaces inside the drop are isothermal. The energy equation (17) may then be suitably recast in terms of the stream function coordinate based on Hill's spherical vortex [13]. The computer time may be reduced to the order of a few seconds.

In Fig. 6, the dimensionless quantities $\bar{q}$ and $\bar{u}_c$ are plotted as functions of time for a vertically falling drop introduced with an initial velocity, $U_0 = 10\,\text{m s}^{-1}$. The far-stream thermodynamic conditions are taken to be prescribed. In the immediate transient period following the introduction, both $\bar{q}$ and $\bar{u}_c$ are very high because of the larger thermal driving force. With increasing time, both the surface and bulk temperatures increase. The internal circulation in the drop is vigorous and provides an efficient mechanism for heat transfer. The thermal driving force keeps getting weaker. Eventually the drop thermalizes with the outside and the condensation ceases. Owing to the smaller heat capacity, the smaller drops equilibrate with the outside sooner than the larger drops. In this figure, we have provided the time histories for $\bar{u}_c$ and $\bar{q}$ as derived both from the complete numerical solution of both flow and transport equations and from employing our correlation in the numerical computations. The predicted results agree very well. This lends credibility to the use of our correlations in predicting condensation heat and mass transfer.

The effect of droplet spray angle on the heat transfer of a liquid drop is shown in Fig. 7. For a given drop size, the rate of rise in bulk temperature θ_b with time is essentially independent of the spray angle. However, the drop vertical-fall height H (in meters) before thermal equilibration is achieved changes significantly with the spray angle. The drop that is introduced in a horizontal direction ($\beta = 90°\text{C}$) experiences considerable heat exchange while essentially in horizontal motion. The fall height is much shorter compared to a drop introduced at any other angle. The design of direct-contact heat and mass transfer equipment will benefit from such data [20].

The rate of drop growth is examined in Fig. 8 through a plot of dimensionless radius $\hat{R}$ with t. The dimensionless growth rate for the drop is given by

$$\frac{1}{\hat{R}}\frac{d\hat{R}}{dt} = -\frac{D_{12}}{2\alpha_1}\frac{\rho_g}{\rho_l}\bar{u}_c. \tag{40}$$

The growth rate increases linearly with the temperature differential $\Delta T = T_\infty - T_0$. The predicted drop size at the end of the condensation is in agreement with equation (28) of ref. [13]. Since the drop growth

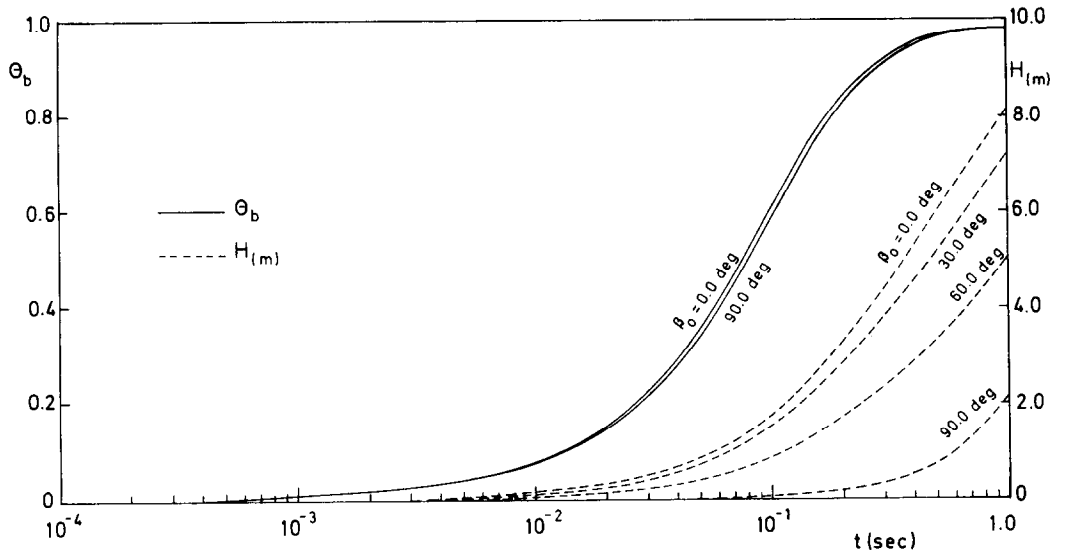

FIG. 7. The effect of droplet spray angle on the variation of bulk temperature and drop vertical-fall height with time. $p_\infty = 300\,\text{kPa}$, $T_\infty = 120°\text{C}$, $U_0 = 15\,\text{m s}^{-1}$, $T_0 = 37°\text{C}$, $R_0 = 250\,\mu\text{m}$, $W_0 = 0.54$.

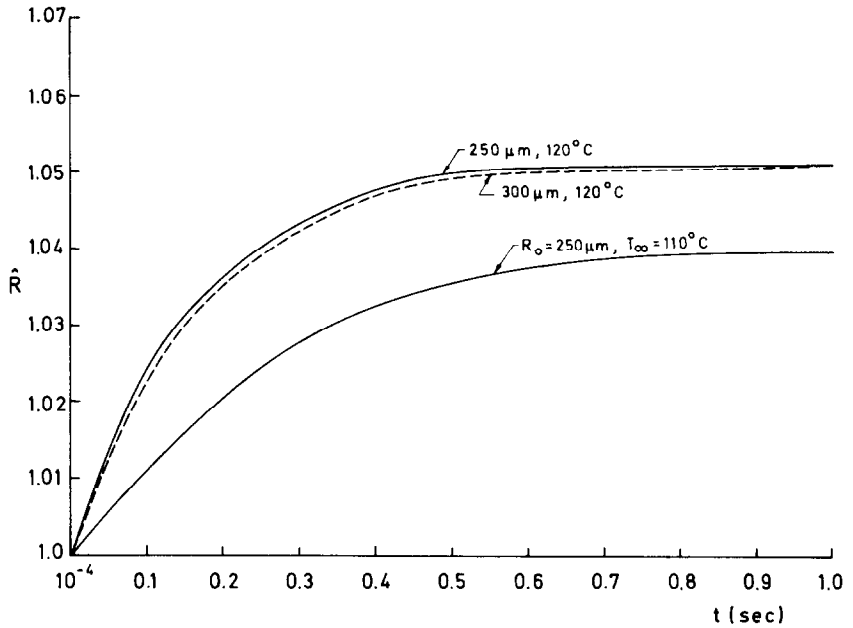

FIG. 8. The drop growth rate. $P_\infty = 300\,\text{kPa}$, $T_0 = 37°\text{C}$, $\beta_0 = 0.0\,\text{deg.}$, $U_0 = 10\,\text{m s}^{-1}$.

rate is intimately connected with the drop heat-up rate, the variation of $\hat{R}$ with ΔT and R_0 can be seen as a direct consequence of the manner in which the temperature profile inside the drop evolves in time.

9. CONCLUSIONS

New correlations for the average condensation velocity and heat flux associated with condensation on a moving liquid drop in the presence of a noncondensable have been provided. The correlations are based on a detailed numerical study that includes transient effects. The formulation in this study entails a simultaneous solution of the partial differential equations that describe the flow field and transport in the gaseous and liquid phases. The correlations presented in this paper are thought to be of considerable usefulness in the design of direct-contact heat/mass transfer equipment.

Acknowledgements—The authors wish to acknowledge gratefully the NSF Grant ECS-8515068 for Super-computer time on CRAY 1A machine and the Super-computer Center at A.T. & T. Bell Laboratories where some detailed computations were carried out.

REFERENCES

1. R. Clift, J. R. Grace and M. E. Weber, *Bubbles, Drops and Particles*. Academic Press, New York (1978).
2. H. R. Jacobs and D. S. Cook, Direct contact condensation on a non-circulating drop, 6th Int. Heat Transfer Conf., Vol. 2, pp. 389–393, Toronto, Ontario (1978).
3. Y. S. Lou and L. S. Yang, Quasi-steady theory of non-equilibrium droplet evaporation and condensation, *J. Appl. Phys.* **50,** 5331–5338 (1978).
4. I. Kh. Rakhmatulina, Nonsteady evaporation and growth of drops in gas(eous) medium, *Int. J. Engng Sci.* **19,** 1114–1122 (1981).
5. J. S. Ford and A. Lekic, Rate of growth of drops during condensation, *Int. J. Heat Mass Transfer* **16,** 61–64 (1973).
6. E. Kulic and E. Rhodes, Direct contact condensation from air–steam mixtures on a single droplet, *Can. J. chem. Engng* **55,** 131–137 (1977).
7. E. Kulic and E. Rhodes, Heat transfer rates to moving droplets in air–steam mixtures, 6th Int. Heat Transfer Conf., pp. 464–474, Toronto, Ontario (1978).
8. S. S. Sadhal and P. S. Ayyaswamy, Flow past a liquid drop with a large non-uniform radial velocity, *J. Fluid Mech.* **133,** 65–81 (1983).
9. J. N. Chung, P. S. Ayyaswamy and S. S. Sadhal, Laminar condensation on a moving drop. Part 1. Singular perturbation technique, *J. Fluid Mech.* **139,** 105–130 (1984).
10. J. N. Chung, P. S. Ayyaswamy and S. S. Sadhal, Laminar condensation on a moving drop. Part 2. Numerical solutions, *J. Fluid Mech.* **139,** 131–144 (1984).
11. J. N. Chung and P. S. Ayyaswamy, Laminar condensation heat and mass transfer of a moving drop, *A.I.Ch.E. Jl* **27,** 372–377 (1981).
12. J. N. Chung and P. S. Ayyaswamy, Material removal associated with condensation on a droplet in motion, *Int. J. Multiphase Flow* **7,** 329–342 (1981).
13. T. Sundararajan and P. S. Ayyaswamy, Hydrodynamics and heat transfer associated with condensation on a moving drop: solutions for intermediate Reynolds numbers, *J. Fluid Mech.* **149,** 33–58 (1984).
14. T. Sundararajan and P. S. Ayyaswamy, Heat and mass transfer associated with condensation on a moving drop: solutions for intermediate Reynolds numbers by a boundary layer formation, *Trans. Am. Soc. Mech. Engrs, J. Heat Transfer* **107,** 409–416 (1985).
15. T. Sundararajan and P. S. Ayyaswamy, Numerical evaluation of heat and mass transfer to a moving liquid drop experiencing condensation, *Numer. Heat Transfer* **8**(6), 689–706 (1985).
16. L. J. Huang and P. S. Ayyaswamy, Drag coefficients associated with a liquid drop experiencing condensation, *Trans. Am. Soc. Mech. Engrs, J. Heat Transfer* (1987), in press.
17. N. Frossling, Uber die verdunstung fallenden tropfen, *Gerlands Beitr. Geophys.* **52,** 170–216 (1939).
18. V. M. Semian, Heat transfer from wet air by vapour condensation, *Teploenergetica* **4** (1956).
19. E. Kulic, E. Rhodes and G. Sullivan, Heat transfer rate predictions in condensation on droplets from air–steam mixtures, *Can. J. chem. Engng* **53,** 252–258 (1975).
20. L. J. Huang and P. S. Ayyaswamy, Heat transfer of a nuclear reactor containment spray drop, *Nucl. Engng Des.* (1987), in press.

TRANSFERT DE CHALEUR ET DE MASSE ASSOCIE A LA CONDENSATION D'UNE GOUTTE DE BROUILLARD: UNE ANALYSE

Résumé—L'hydrodynamique et le transfert de chaleur et de masse variables dans le temps et associés à la condensation sur une goutte de brouillard sont étudiés pour le nombre de Reynolds de la goutte dans le domaine $Re = O(100)$. L'environnement de la goutte est un mélange de vapeur saturante et d'incondensable. La formulation est une solution simultanée des équations aux dérivées partielles qui décrivent le champ d'écoulement et le transport dans les phases gazeuse et liquide. La trajectoire de la goutte est déterminée en résolvant les équations de la composition de la force de pesanteur et de la traînée. Des résultats sont donnés pour les variations dans le temps de la température de la goutte, des coefficients aérodynamiques, de la vitesse moyenne de condensation et du flux moyen de chaleur. On discute l'effet de l'angle de pulvérisation sur la hauteur verticale de chute avant d'obtenir l'équilibre thermique avec l'environnement. Les résultats montrent un accord excellent avec les données expérimentales disponibles. On donne de nouvelles formules pour la vitesse moyenne de condensation et pour le flux thermique moyen associé à la condensation sur une goutte liquide mobile, en présence d'un gaz non consensable. Les formules sont très utiles dans le dimensionnement d'un équipement de transfert de chaleur et de masse par contact direct.

WÄRME- UND STOFFTRANSPORT BEI DER SPRÜHTROPFENKONDENSATION— EINE VOLLSTÄNDIGE INSTATIONÄRE BERECHNUNG

Zusammenfassung—Es wurde die zeitabhängige Strömung und der Wärme- und Stofftransport bei der Kondensation an einem Sprühtropfen bei Reynolds-Zahlen der Größenordnung $Re = 100$ untersucht. Die Umgebung des Tropfens ist ein Gemisch aus gesättigtem Dampf und einem nichtkondensierbaren Gas. Die Beschreibung enthält eine simultane Lösung der partiellen Differentialgleichungen, welche das Strömungsfeld und den Wärme- und Stofftransport in der gasförmigen und flüssigen Phase beschreiben. Die Tropfenbahn erhält man durch Lösung der Bilanzgleichungen für die Schwerkraft und die Widerstandskraft. Es werden Ergebnisse gezeigt für zeitliche Änderungen der Tropfenmitteltemperatur, für verschiedene Widerstandskoeffizienten, mittlere Kondensationsgeschwindigkeiten und mittlere Wärmestromdichten. Es wird der Einfluß des Sprühwinkels auf die Tropfenfallhöhe bis zum Erreichen des thermischen Gleichgewichts mit der äußeren Umgebung diskutiert. Die Ergebnisse zeigen sehr gute Übereinstimmung mit experimentellen Daten—soweit verfügbar. Es werden neue Korrelationen für die mittlere Kondensationsgeschwindigkeit und die mittlere Wärmestromdichte bei der Kondensation an einem sich bewegenden Flüssigkeitstropfen in Gegenwart eines nicht kondensierbaren Gases vorgeschlagen. Die Korrelationen sollten von guter Brauchbarkeit für die Auslegung von Wärme- und Stoffübertragungsanlagen mit direktem Kontakt der Medien sein.

ТЕПЛО- И МАССОПЕРЕНОС, СВЯЗАННЫЙ С КОНДЕНСАЦИЕЙ НА КАПЛЕ ПРИ РАСПЫЛЕ: АНАЛИЗ ПЕРЕХОДНОГО РЕЖИМА

Аннотация—Нестационарный тепло- и массоперенос, обусловленный конденсацией на капле при распыле, исследуется для чисел Рейнольдса движения капли $Re = O(100)$. Капля окружена смесью насыщенного и конденсирующегося пара. Одновременно решаются дифференциальные уравнения в частных производных, описывающие поле течения и перенос в газовых и жидких фазах. Траектория движения капли определяется из баланса сил тяжести и торможения. Результаты получены для зависящей от времени среднемассовой температуры капли, различных коэффициентов торможения, осредненных скорости конденсации и теплового потока. Обсуждается влияние угла распыла на путь, проходимый каплей при вертикальном падении, до достижения ею теплового равновесия с окружающей средой. Результаты хорошо согласуются с имеющимися экспериментальными данными. Представлены новые зависимости для осредненных скорости конденсации и теплового потока, связанных с конденсацией на движущейся капле жидкости в присутствии неконденсирующегося пара. Предполагается, что эти зависимости найдут применение при проектировании тепломассообменного оборудования.